Detectability of patches in fractal textures

for assessing Hölder exponent-based breast cancer risk evaluation

Journées MISTIC

Lyon

May 26, 2025

Barbara Pascal

Laboratoire des Sciences du Numérique de Nantes: B. Pascal

Institut Denis Poisson: H. Biermé

Thank you MISTIC!

Context and motivations

Breast cancer:

- most common cancer amongst women with ~ 1 over 8 diagnosed in her life
- early detection is critical for the patient's survival

Breast cancer:

- most common cancer amongst women with ~ 1 over 8 diagnosed in her life
- early detection is critical for the patient's survival

X-ray imaging: most used imaging technique yielding a so-called *mammogram*

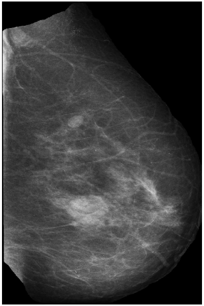

Mammogram provided by **CompUMaine** (Gerasimova-Chechkina et al., 2021, *Front. Physiol.*)

Breast cancer:

- most common cancer amongst women with $\sim$ 1 over 8 diagnosed in her life
- early detection is critical for the patient's survival

X-ray imaging: most used imaging technique yielding a so-called *mammogram*

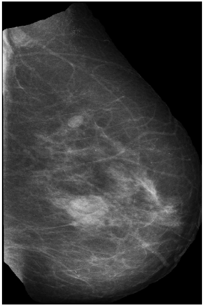

Assessment by a radiologist:

- fatty tissues: translucent to X-rays (black)
- epithelial and stromal tissues: absorb X-rays (white)
- tumorous tissues: **also absorb X-rays** (white)

$\Longrightarrow$ errors of both I and II types

Mammogram provided by **CompUMaine** (Gerasimova-Chechkina et al., 2021, *Front. Physiol.*)

Breast cancer:

- most common cancer amongst women with $\sim$ 1 over 8 diagnosed in her life
- early detection is critical for the patient's survival

X-ray imaging: most used imaging technique yielding a so-called *mammogram*

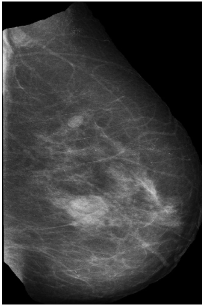

Assessment by a radiologist:

- fatty tissues: translucent to X-rays (black)
- epithelial and stromal tissues: absorb X-rays (white)
- tumorous tissues: **also absorb X-rays** (white)

$\Longrightarrow$ errors of both I and II types

Mammogram provided by **CompUMaine** (Gerasimova-Chechkina et al., 2021, *Front. Physiol.*)

Computer-Aided Detection: used in 92% of screening mammograms in the U.S.

Self-similar isotropic random fields: $\forall c > 0$

$$\{\mathsf{F}(c\underline{x}); \underline{x} \in \mathbb{R}^2\} \overset{\text{(law)}}{=} c^H \{\mathsf{F}(\underline{x}); \underline{x} \in \mathbb{R}^2\}$$

$h(\underline{x})$: *local Hölder exponent* $\equiv H \in (0, 1)$

Mammogram

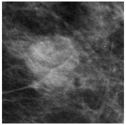

fractal random field

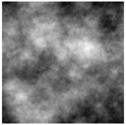

Self-similar isotropic random fields: $\forall c > 0$

$$\{\mathsf{F}(c\underline{x}); \underline{x} \in \mathbb{R}^2\} \overset{\text{(law)}}{=} c^H \{\mathsf{F}(\underline{x}); \underline{x} \in \mathbb{R}^2\}$$

$h(\underline{x})$: *local Hölder exponent* $\equiv H \in (0, 1)$

Mammogram

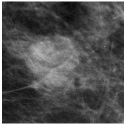

fractal random field

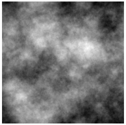

Fractal analysis applied to mammograms: e.g., fractal dimension of a rough surface

- characterization of mammogram density (Caldwell et al., 1990, *Phys. Med. Biol.*)
- lesion detection in mammograms (Burgess et al., 2001, *Med. Biol.*; Zebari et al., 2021, *Appl. Sci.*)
- assessment of breast cancer risk (Heine et al., 2002, *Acad. Radiol.*; Marin et al., 2017, *Med. Phys.*; Gerasimova-Chechkina et al., 2021, *Front. Physiol.*)

Fractal analysis tools in medical imaging

Self-similar isotropic random fields: $\forall c > 0$

$$\{F(c\underline{x}); \underline{x} \in \mathbb{R}^2\} \overset{\text{(law)}}{=} c^H \{F(\underline{x}); \underline{x} \in \mathbb{R}^2\}$$

$h(\underline{x})$: *local Hölder exponent* $\equiv H \in (0,1)$

Mammogram

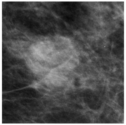

fractal random field

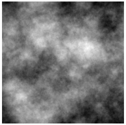

Fractal analysis applied to mammograms: e.g., fractal dimension of a rough surface

- characterization of mammogram density (Caldwell et al., 1990, *Phys. Med. Biol.*)
- lesion detection in mammograms (Burgess et al., 2001, *Med. Biol.*; Zebari et al., 2021, *Appl. Sci.*)
- assessment of breast cancer risk (Heine et al., 2002, *Acad. Radiol.*; Marin et al., 2017, *Med. Phys.*; Gerasimova-Chechkina et al., 2021, *Front. Physiol.*)

And beyond in medical imaging: (Biermé et al., 2009, *Proc. ESAIM*)

- characterization of osteoporosis in X-ray images of bones (Benhamou et al., 2001, *J. Bone Miner. Res.*; Cui et al., 2023, *Front. Bioeng. Biotechnol.*)
- morphological evaluation of white matter in brain magnetic resonance images (Shan et al., 2006, *Magn. Reson. Imaging*)

Fractal analysis tools in medical imaging

Self-similar isotropic random fields: $\forall c > 0$

$$\{\mathrm{F}(c\underline{x}); \underline{x} \in \mathbb{R}^2\} \stackrel{(\mathrm{law})}{=} c^H \{\mathrm{F}(\underline{x}); \underline{x} \in \mathbb{R}^2\}$$

$h(\underline{x})$: *local Hölder exponent* $\equiv H \in (0, 1)$

Mammogram

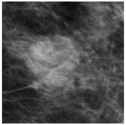

fractal random field

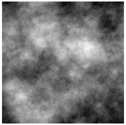

Tissue characterization based on *local Hölder exponent*:

fatty tissues

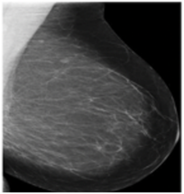

$H_{\mathrm{b}} \simeq 0.30$

healthy **dense** tissues

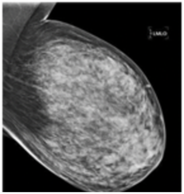

$H_{\mathrm{b}} \simeq 0.65$

(Kestener et al., 2001, *Image Anal. Stereol.*;

Self-similar isotropic random fields: $\forall c > 0$

$$\{F(c\underline{x}); \underline{x} \in \mathbb{R}^2\} \overset{(\text{law})}{=} c^H \{F(\underline{x}); \underline{x} \in \mathbb{R}^2\}$$

$h(\underline{x})$: *local Hölder exponent* $\equiv H \in (0, 1)$

Mammogram

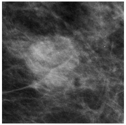

fractal random field

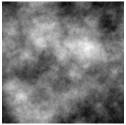

Tissue characterization based on *local Hölder exponent*:

fatty tissues

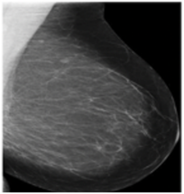

$H_{\mathrm{b}} \simeq 0.30$

disrupted tissues

$H_{\mathrm{p}} \simeq 0.5$

$\Longrightarrow$ breast cancer risk

healthy **dense** tissues

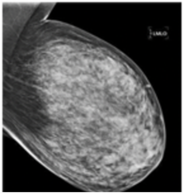

$H_{\mathrm{b}} \simeq 0.65$

(Kestener et al., 2001, *Image Anal. Stereol.*; Marin et al., 2017, *Med. Phys.*; Gerasimova-Chechkina et al., 2021, *Front. Physiol.*)

Synthetic isotropic fractal textures

Self-similar Gaussian fields: $\forall c > 0, \{\mathsf{F}(c\underline{x}); \underline{x} \in \mathbb{R}^2\} \overset{(\text{law})}{=} c^H \{\mathsf{F}(\underline{x}); \underline{x} \in \mathbb{R}^2\},\ H \in (0,1)$

- computer vision (Ilow et al., 2001, *IEEE Trans. Image Process.*)
- stochastic geometry (Biermé et al., 2009, *Proc. ESAIM*; Cohen & Istas, 2013, *Spinger*)
- turbulent fluid mechanics (Pereira, et al., 2016, *J. Fluid Mech.*)

Self-similar Gaussian fields: $\forall c > 0, \{\mathsf{F}(c\underline{x}); \underline{x} \in \mathbb{R}^2\} \overset{(\text{law})}{=} c^H \{\mathsf{F}(\underline{x}); \underline{x} \in \mathbb{R}^2\},\ H \in (0,1)$

- computer vision (Ilow et al., 2001, *IEEE Trans. Image Process.*)
- stochastic geometry (Biermé et al., 2009, *Proc. ESAIM*; Cohen & Istas, 2013, *Spinger*)
- turbulent fluid mechanics (Pereira, et al., 2016, *J. Fluid Mech.*)

*F*ractional *B*rownian *f*ield (B. B. Mandelbrot & J. W. Van Ness, 1968, *SIAM Rev.*)

$$\mathsf{B}_H(\underline{x}) = \int_{\mathbb{R}^2} \frac{\mathrm{e}^{-\mathrm{i}\underline{x}\cdot\underline{\omega}} - 1}{\|\underline{\omega}\|^{H+1}} \mathrm{d}\widetilde{\mathrm{W}}(\underline{\omega}), \quad \text{Hurst exponent } H \in (0,1)$$

Stationary isotropic self-similar textures:

*F*ractional *G*aussian *f*ield (B. Pascal et al., 2021, *Appl. Comput. Harmon. Anal.*)

$$\mathsf{G}_H(\underline{x}) = \frac{1}{2}\left(\mathsf{B}_H(\underline{x} + \underline{e}_1) + \mathsf{B}_H(\underline{x} + \underline{e}_2) - 2\mathsf{B}_H(\underline{x})\right)$$

Filtered fractional Brownian field

$$\mathsf{C}_H(\underline{x}) = \langle \mathsf{B}_H, \mathsf{u}_{\underline{x}} \rangle, \text{ u } \textbf{isotropic} \text{ high-pass filter, } \langle \cdot, \cdot \rangle \text{ scalar product in } L^2(\mathbb{R}^2)$$

Design of filter u inspired by (Biermé et al., 2024, *Preprint*)

Self-similar fields: two **stationary** texture models

fBf $\quad \mathrm{B}_H(\underline{x}) = \int_{\mathbb{R}^2} \frac{\mathrm{e}^{-\mathrm{i}\underline{x}\cdot\underline{\omega}} - 1}{\|\underline{\omega}\|^{H+1}} \, \mathrm{d}\widetilde{\mathrm{W}}(\underline{\omega}),$ Hurst exponent $H \in (0,1)$

fGf $\quad \mathrm{G}_H(\underline{x}) = \frac{1}{2}\left(\mathrm{B}_H(\underline{x} + \underline{e}_1) + \mathrm{B}_H(\underline{x} + \underline{e}_2) - 2\mathrm{B}_H(\underline{x})\right)$

Filtered fBf $\quad \mathrm{C}_H(\underline{x}) = \langle \mathrm{B}_H, \mathrm{u}_{\underline{x}} \rangle$, u isotropic high-pass filter

Examples: *left:* $H = 0.3 \sim$ fatty tissues; *right:* $H = 0.65 \sim$ healthy dense tissues

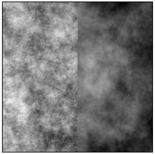

fBf B_H

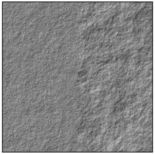

fGf G_H

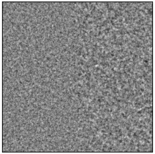

Filtered fBf

Detectability of disrupted tissues depending on microenvironment

Background: healthy microenvironment

- fatty: $H_\mathrm{b} = 0.3$ (anticorrelated)
- dense: $H_\mathrm{b} = 0.65$ (correlated)

Patch: disrupted tissues

- $H_\mathrm{p} = 0.5$ (uncorrelated)

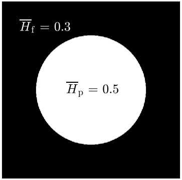

Fatty background

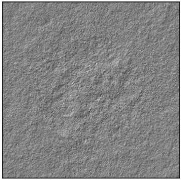
fGf

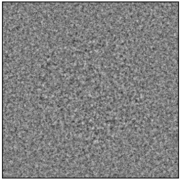
Filtered fBf

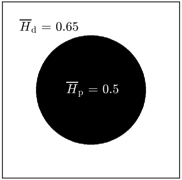

Dense background

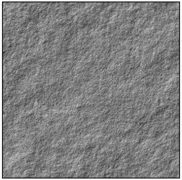
fGf

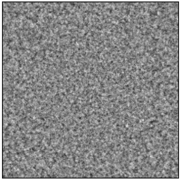
Filtered fBf

Field $\mathsf{F} : \mathbb{R}^2 \to \mathbb{R}$, *local Hölder exponent* at $\underline{x}_0$ largest $\alpha > 0$ such that

$$\forall \underline{x} \in \mathcal{V}(\underline{x}_0), \quad |\mathsf{F}(x) - \mathcal{P}_{\underline{x}_0}(\underline{x})| \leq \chi \|\underline{x} - \underline{x}_0\|^{\alpha}, \quad \chi > 0$$

with $\mathcal{P}_{\underline{x}_0}$ a polynomial of degree lower than α.

B_H, G_H and C_H: $\forall \underline{x} \in \mathbb{R}^2$, $h(\underline{x}) = H$.

Self-similarity index and local Hölder exponent

Field $\mathsf{F} : \mathbb{R}^2 \to \mathbb{R}$, *local Hölder exponent* at $\underline{x}_0$ largest $\alpha > 0$ such that

$$\forall \underline{x} \in \mathcal{V}(\underline{x}_0), \quad |\mathsf{F}(x) - \mathcal{P}_{\underline{x}_0}(\underline{x})| \leq \chi \|\underline{x} - \underline{x}_0\|^{\alpha}, \quad \chi > 0$$

with $\mathcal{P}_{\underline{x}_0}$ a polynomial of degree lower than α.

B_H, G_H and C_H: $\forall \underline{x} \in \mathbb{R}^2$, $h(\underline{x}) = H$.

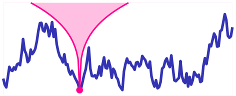

$H = 0.3$

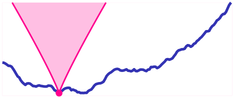

$H = 0.65$

Examples: *left:* $H = 0.3 \sim$ fatty tissues; *right:* $H = 0.65 \sim$ healthy dense tissues

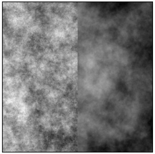

fBf B_H

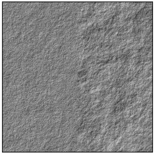

fGf G_H

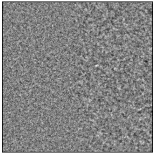

Filtered fBf

Multiscale Analysis via Wavelet Leader Coefficients

Decimated Wavelet Transform: field $\mathsf{F} : \mathbb{R}^2 \to \mathbb{R}$ (Mallat, 1999, *Elsevier*)

$$\text{scaling function } \phi, \text{ mother wavelet } \psi \Longrightarrow \mathcal{Y}_{\mathsf{F}}^{(m)}(j, \underline{k}) = 2^{-j} \langle \mathsf{F}, \psi_{j,\underline{k}}^{(m)} \rangle \ ;$$

Decimated Wavelet Transform: field $\mathsf{F} : \mathbb{R}^2 \to \mathbb{R}$ (Mallat, 1999, *Elsevier*)

$$\text{scaling function } \phi, \text{ mother wavelet } \psi \Longrightarrow \mathcal{Y}_{\mathsf{F}}^{(m)}(j, \underline{k}) = 2^{-j} \langle \mathsf{F}, \psi_{j,\underline{k}}^{(m)} \rangle \ ;$$

Wavelet leaders: (Jaffard, 2004, *Proc. Symp. Pure Math.*)

$$\mathcal{L}_{j,\underline{k}} = \sup\{ |2^j \mathcal{Y}_{j',\underline{k}'}^{(m)}|, \ \lambda_{j',\underline{k}'} \subset 3\lambda_{j,\underline{k}}, m = 1,2,3\}$$

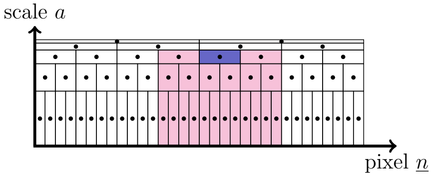

Decimated Wavelet Transform: field $\mathsf{F} : \mathbb{R}^2 \to \mathbb{R}$ (Mallat, 1999, *Elsevier*)

$$\text{scaling function } \phi,\ \text{mother wavelet } \psi \Longrightarrow \mathcal{Y}_{\mathsf{F}}^{(m)}(j, \underline{k}) = 2^{-j}\langle \mathsf{F}, \psi_{j,\underline{k}}^{(m)} \rangle \ ;$$

Wavelet leaders: (Jaffard, 2004, *Proc. Symp. Pure Math.*)

$$\mathcal{L}_{j,\underline{k}} = \sup\{|2^j \mathcal{Y}_{j',\underline{k}'}^{(m)}|,\ \lambda_{j',\underline{k}'} \subset 3\lambda_{j,\underline{k}},\ m = 1, 2, 3\}$$

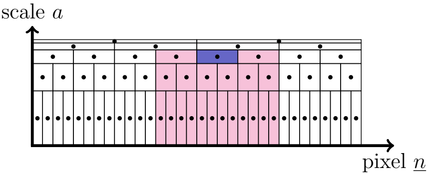

$$\mathcal{L}_{j,\underline{k}} \simeq \eta(\underline{x}) 2^{jh(\underline{x})} \quad \text{as} \quad 2^j \to 0$$

(Jaffard, 2004, *Proc. Symp. Pure Math.*)

Decimated Wavelet Transform: field $\mathsf{F} : \mathbb{R}^2 \to \mathbb{R}$ (Mallat, 1999, *Elsevier*)

$$\text{scaling function } \phi, \text{ mother wavelet } \psi \Longrightarrow \mathcal{Y}_{\mathsf{F}}^{(m)}(j, \underline{k}) = 2^{-j} \langle \mathsf{F}, \psi_{j,\underline{k}}^{(m)} \rangle \ ;$$

Wavelet leaders: (Jaffard, 2004, *Proc. Symp. Pure Math.*)

$$\mathcal{L}_{j,\underline{k}} = \sup\{ |2^j \mathcal{Y}_{j',\underline{k}'}^{(m)}|, \ \lambda_{j',\underline{k}'} \subset 3\lambda_{j,\underline{k}}, m = 1, 2, 3\}$$

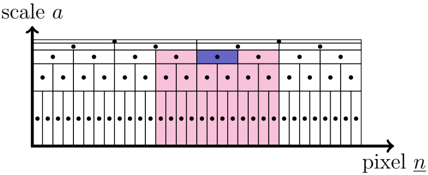

$$\mathcal{L}_{j,\underline{k}} \simeq \eta(\underline{x}) 2^{jh(\underline{x})} \quad \text{as} \quad 2^j \to 0$$

(Jaffard, 2004, *Proc. Symp. Pure Math.*)

Textured image

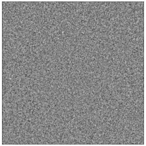

$a = 2^1$

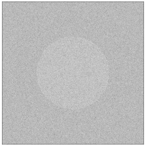

$a = 2^2$

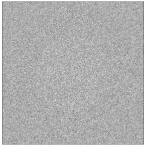

. . .

$a = 2^7$

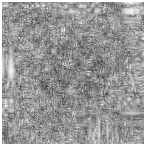

Multiscale Analysis via Wavelet Leader Coefficients

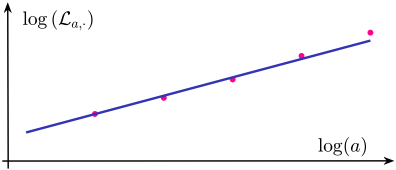

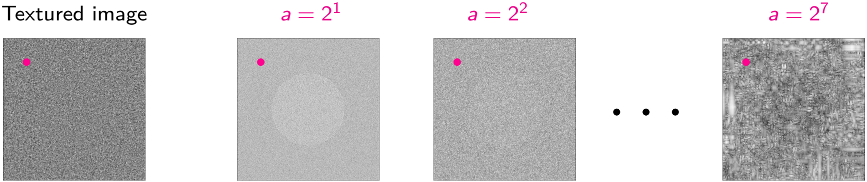

Multiscale Analysis via Wavelet Leader Coefficients

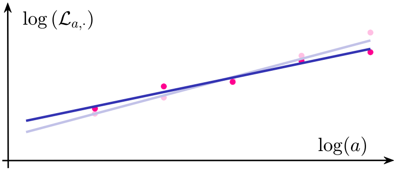

Textured image

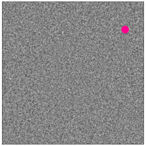

$a = 2^1$

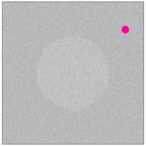

$a = 2^2$

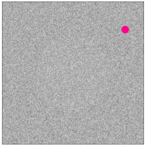

$\cdots$

$a = 2^7$

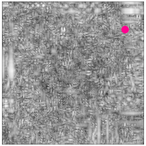

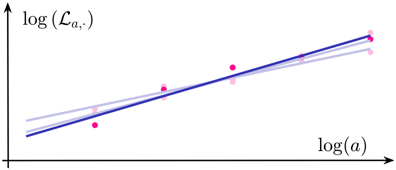

$\log(\mathcal{L}_{a,\cdot})$
$\log(a)$

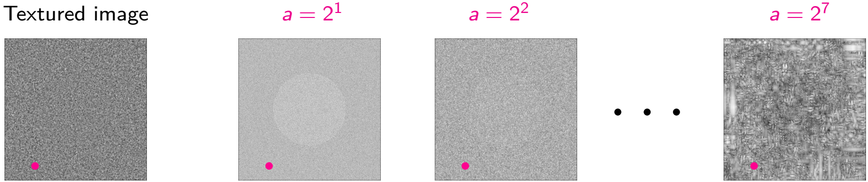

Textured image
$a = 2^1$
$a = 2^2$
$\cdots$
$a = 2^7$

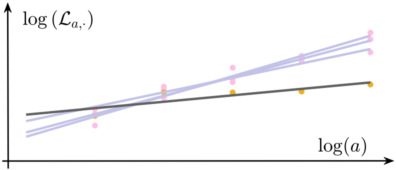

Textured image

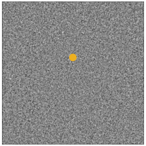

$a = 2^1$

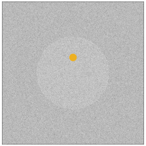

$a = 2^2$

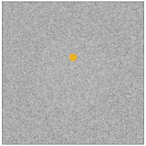

...

$a = 2^7$

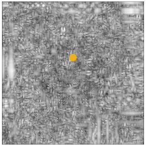

Multiscale Analysis via Wavelet Leader Coefficients

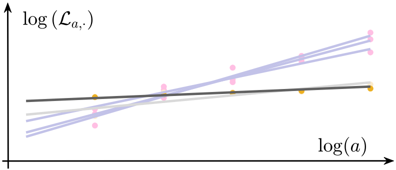

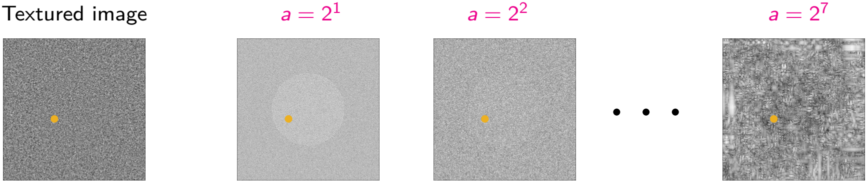

Multiscale Analysis via Wavelet Leader Coefficients

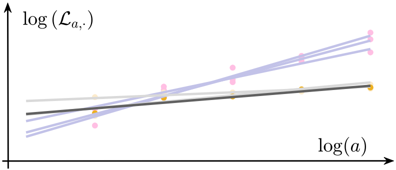

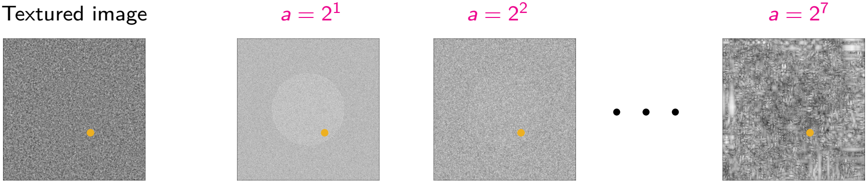

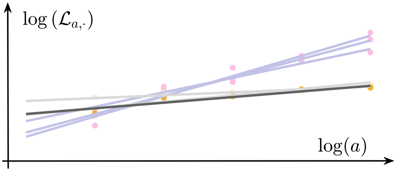

True $\overline{\boldsymbol{h}}$

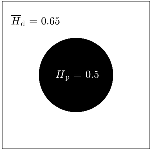

Lin. reg. $\widehat{\boldsymbol{h}}^{\mathrm{LR}}$

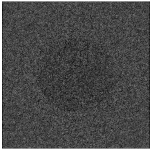

Textured image

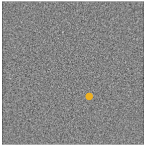

$a = 2^1$

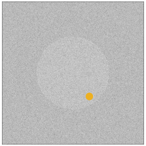

$a = 2^2$

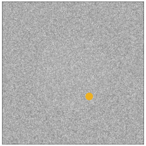

$\cdots$

$a = 2^7$

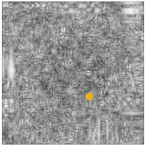

Regularized Estimate of Local Regularity

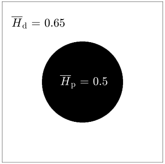

True $\overline{\boldsymbol{h}}$

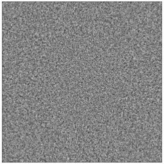

Piecewise texture

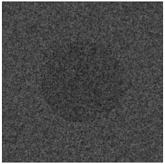

Lin. reg. $\widehat{\boldsymbol{h}}^{\mathrm{LR}}$

Threshold Rudin-Osher-Fatemi estimator: **D**: 2D discrete gradients

$$\widehat{\boldsymbol{h}}^{\mathsf{ROF}} = \operatorname{argmin}_{\boldsymbol{h}} \|\boldsymbol{h} - \widehat{\boldsymbol{h}}^{\mathsf{LR}}\|_2^2 + \lambda \|\mathbf{D}\boldsymbol{h}\|_{2,1}$$

(Nelson et al., 2016, *IEEE Trans. Image Process.*; B. Pascal et al., 2018, *ICASSP*; Cai et al., 2013, SIAM J. Imaging Sci.; Pascal et al., 2021, Appl. Comput. Harm. Anal.)

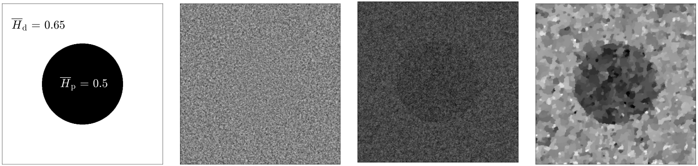

True $\overline{\boldsymbol{h}}$ | Piecewise texture | Lin. reg. $\widehat{\boldsymbol{h}}^{\mathsf{LR}}$ | ROF $\widehat{\boldsymbol{h}}^{\mathsf{ROF}}$

Regularized Estimate of Local Regularity

Threshold Rudin-Osher-Fatemi estimator: **D**: 2D discrete gradients

$$\widehat{\boldsymbol{h}}^{\mathrm{ROF}} = \operatorname{argmin}_{\boldsymbol{h}} \|\boldsymbol{h} - \widehat{\boldsymbol{h}}^{\mathrm{LR}}\|_2^2 + \lambda \|\mathbf{D}\boldsymbol{h}\|_{2,1}$$

& iterative thresholding $\Longrightarrow \mathcal{T}\widehat{\boldsymbol{h}}^{\mathrm{ROF}}$ (Nelson et al., 2016, *IEEE Trans. Image Process.*; B. Pascal et al., 2018, *ICASSP*; Cai et al., 2013, SIAM J. Imaging Sci.; Pascal et al., 2021, Appl. Comput. Harm. Anal.)

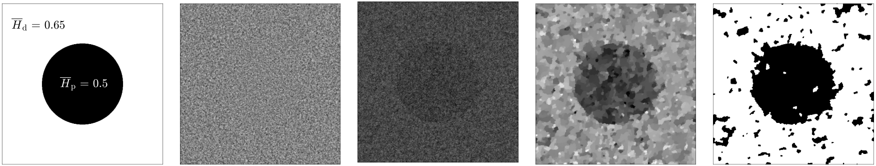

True $\overline{\boldsymbol{h}}$ | Piecewise texture | Lin. reg. $\widehat{\boldsymbol{h}}^{\mathrm{LR}}$ | ROF $\widehat{\boldsymbol{h}}^{\mathrm{ROF}}$ | T-ROF $\mathcal{T}\widehat{\boldsymbol{h}}^{\mathrm{ROF}}$

Threshold Rudin-Osher-Fatemi estimator: $\mathbf{D}$: 2D discrete gradients

$$\widehat{\boldsymbol{h}}^{\mathrm{ROF}} = \operatorname{argmin}_{\boldsymbol{h}} \|\boldsymbol{h} - \widehat{\boldsymbol{h}}^{\mathrm{LR}}\|_2^2 + \lambda \|\mathbf{D}\boldsymbol{h}\|_{2,1}$$

& iterative thresholding $\Longrightarrow \mathcal{T}\widehat{\boldsymbol{h}}^{\mathrm{ROF}}$ (Nelson et al., 2016, *IEEE Trans. Image Process.*; B. Pascal et al., 2018, *ICASSP*; Cai et al., 2013, SIAM J. Imaging Sci.; Pascal et al., 2021, Appl. Comput. Harm. Anal.)

Stein-based automated parameter tuning: Generalized Stein Unbiased Risk Estimate

$$\mathsf{GSURE}(\lambda) = \|\widehat{\boldsymbol{h}}^{\mathrm{ROF}} - \widehat{\boldsymbol{h}}^{\mathrm{LR}}\|^2 + 2\mathrm{Tr}\left(\boldsymbol{\mathcal{S}}\boldsymbol{J}\right) - \mathrm{Tr}(\boldsymbol{\mathcal{S}})$$ not explicitly depending on $\overline{\boldsymbol{h}}$

$\boldsymbol{J}$: Jacobian of $\widehat{\boldsymbol{h}}^{\mathrm{ROF}}$ w.r.t. $\widehat{\boldsymbol{h}}^{\mathrm{LR}}$; $\boldsymbol{\mathcal{S}}$: empirical covariance of Gaussian noise in $\widehat{\boldsymbol{h}}^{\mathrm{LR}}$

$\mathsf{GSURE}(\lambda) \approx \|\widehat{\boldsymbol{h}}^{\mathrm{ROF}} - \overline{\boldsymbol{h}}\|_2^2 \Longrightarrow \lambda^\star$: minimization of $\mathsf{GSURE}(\lambda)$ with a BFGS scheme (Pascal et al., 2020, Ann. Telecommun.)

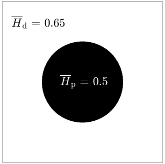

True $\overline{\boldsymbol{h}}$

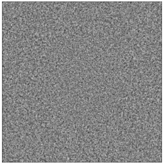
Piecewise texture

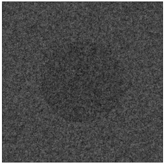
Lin. reg. $\widehat{\boldsymbol{h}}^{\mathrm{LR}}$

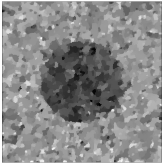
ROF $\widehat{\boldsymbol{h}}^{\mathrm{ROF}}$

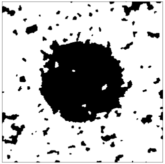
T-ROF $\mathcal{T}\widehat{\boldsymbol{h}}^{\mathrm{ROF}}$

Detectability of disrupted tissues

Detection performance criteria: F-score $F_1^{-1} = \text{precision}^{-1} + \text{recall}^{-1}$

- precision: proportion of pixels segmented in the central patch belonging to it;
- recall: proportion of pixels belonging to the central patch correctly segmented.

$\Longrightarrow$ The larger $F_1 \in [0, 1]$ the better in terms of both types I and II errors.

Detection performance criteria: F-score $F_1^{-1} = \text{precision}^{-1} + \text{recall}^{-1}$

- precision: proportion of pixels segmented in the central patch belonging to it;
- recall: proportion of pixels belonging to the central patch correctly segmented.

$\Longrightarrow$ The larger $F_1 \in [0, 1]$ the better in terms of both types I and II errors.

Patch of disrupted tissues embedded in *fatty* (top) vs. *dense* (bottom) background

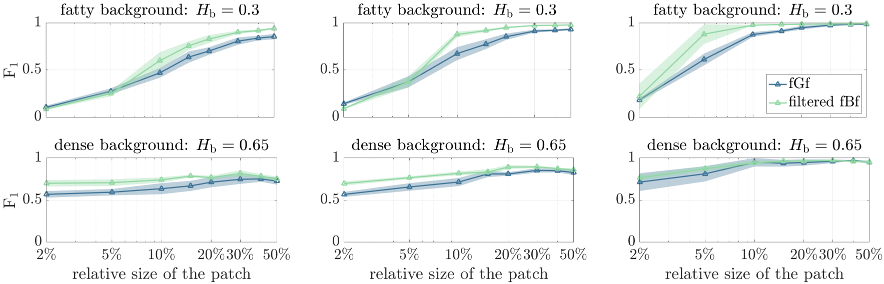

$N = 256$ $N = 512$ $N = 1024$

▶ average and 95% confidence regions computed on 10 texture realizations.

Detectability of disrupted tissues

Detection performance criteria: F-score $F_1^{-1} = \text{precision}^{-1} + \text{recall}^{-1}$

- precision: proportion of pixels segmented in the central patch belonging to it;
- recall: proportion of pixels belonging to the central patch correctly segmented.

$\Longrightarrow$ The larger $F_1 \in [0, 1]$ the better in terms of both types I and II errors.

Patch of disrupted tissues embedded in *fatty* (top) vs. *dense* (bottom) background

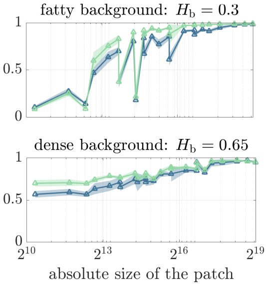

All resolutions

▶ average and 95% confidence regions computed on 10 texture realizations.

Contributions:

- *Filtered f*ractional *B*rownian *f*ield model for stationary isotropic fractal textures.
- Disrupted patch detection in synthetic *filtered fBf* and fractional Gaussian Fields.
- Quantification of the detectability of simulated disrupted tissues $H_\mathrm{p} = 0.5$ in

  simulated fatty $H_\mathrm{b} = 0.3$ vs. dense $H_\mathrm{b} = 0.65$ tissues.

Outcomes:

- High performance for large patches in **fatty** environments, but rapid drop.
- In **dense** environments: good performance, decrease slowly with patch size.

Perspectives:

- Disrupted tissues in *anistropic* textures (Richard & Biermé, 2010, *J. Math. Imaging Vis.*),
- Confidence level on risk cancer assessment on real datasets: VinDr-Mammo.